

Article

Simple-Yet-Effective SRTM DEM Improvement Scheme for Dense Urban Cities Using ANN and Remote Sensing Data: Application to Flood Modeling

Dong Eon Kim ^{1,*}, Shie-Yui Liong ¹, Philippe Gourbesville ², Ludovic Andres ³ and Jiandong Liu ¹

¹ Tropical Marine Science Institute, National University of Singapore, Singapore 119227, Singapore; tmslsy@nus.edu.sg (S-Y.L.); tmsliuj@nus.edu.sg (J.L.)

² Polytech Lab, University of Nice Sophia Antipolis, 06100 Nice, France; Philippe.Gourbesville@unice.fr

³ Métropole Nice Côte d'Azur, 06000 Nice, France; ludovic.andres@nicedotedazur.org

* Correspondence: tmskde@nus.edu.sg

Received: 30 December 2019; Accepted: 11 March 2020; Published: 14 March 2020



Abstract: Digital elevation models (DEMs) are crucial in flood modeling as DEM data reflects the actual topographic characteristics where water can flow in the model. However, a high-quality DEM is very difficult to acquire as it is very time consuming, costly, and, often restricted. DEM data from a publicly accessible satellite, Shuttle Radar Topography Mission (SRTM), and Sentinel 2 multispectral imagery are selected and used to train the artificial neural network (ANN) to improve the quality of SRTM's DEM. High-quality DEM is used as target data in the training of ANN. The trained ANN will then be ready to efficiently and effectively generate a high-quality DEM, at low cost, for places where ground truth DEM data is not available. In this paper, the performance of the DEM improvement scheme is evaluated over two dense urban cities, Nice (France) and Singapore; with the performance criteria using various matrices, e.g., visual clarity, scatter plots, root mean square error (RMSE) and flood maps. The DEM resulting from the improved SRTM (iSRTM) showed significantly better results than the original SRTM DEM, with about 38% RMSE reduction. Flood maps from iSRTM DEM show much more reasonable flood patterns than SRTM DEM's flood map.

Keywords: artificial neural network; digital elevation model; improved SRTM; remote sensing

1. Introduction

Accurate terrain elevation information is important in many applications of land surface modeling, such as flood, volcanology, ecology, and glaciology modeling [1–3]. Space-borne radar or air-borne laser scanning are widely applied to retrieve data on topography that is used to develop the digital elevation model (DEM) [4–6]. A DEM can be used to depict the terrain of the earth and is an organized array of the numbers which represent the elevations of spatial distributions above an arbitrary datum [7]. The principle of a DEM is to describe the elevations of various points in a given area in a digital format. The term DEM is usually applied to land surface topography, but it is a general term that is used to depict the spatial patterns of various surfaces, e.g., surface water, ground surface, canopy, and so on. Digital surface model (DSM) and digital terrain model (DTM) are the two other terms which are frequently used for the ground terrain. DTM is referred to as the Earth terrain, i.e., bare ground, while DSM includes objects on the ground such as buildings and trees.

The Shuttle Radar Topography Mission (SRTM) is a publicly accessible DEM, at a global scale. Although it is provided at no cost, its accuracy is limited, with a root mean square error (RMSE) of more than 8 m in Singapore's dense urban/forest areas [8]. It was reported that SRTM suffers from

inaccuracy especially in areas covered by the canopy, as the 5.6 cm wavelength used does not penetrate vegetation well [9]. The absolute vertical SRTM error was found to be 22.35 m across 255,646 samples in the Amazon rainforest [10], whilst in open areas of South America the equivalent error was at 6.2 m [5]. Also, due to the rapid development of the urban area and coarse resolution, SRTM cannot capture the current building characteristics (SRTM collected the radar imagery in 2000 with approximately 30 m resolution) [11,12]. There have been many studies on improving/correcting satellite DEMs using various methods. Data fusion is one of the techniques used for eliminating errors from space-borne DEMs [11,13–15]. Muhadi et al. (2019) used a data fusion technique for deriving DEM that exploits two or more data to create a new data set for the planning and management of an oil farm plantation [16]. The idea is the limitation of one sensor could be compensated by the other sensors, so the combination of different data sets overcome the limitations.

There are other types of studies using artificial neural networks (ANNs) for DEM improvement. Wendi et al. (2016) presented a promising DEM improvement scheme and showed substantial improvement of SRTM DEM with a RMSE reduction of 52–68% over two different forested areas in Singapore [9]. The author used the ANN together with Landsat 8 multispectral imagery and 92 m resolution of SRTM to eliminate the error caused by dense canopy level in original SRTM. The application of ANN to improve SRTM was used in coastal areas where the elevation varies from 1 m to 20 m [17]. The author used various input nodes in ANN which represent the characteristics of terrain such as slope, population density, canopy height, ICESat (Ice, Cloud and Land elevation satellite), and vegetation density. In the testing set, the RMSE between ground truth and derived SRTM were reduced by approximately 50%, and trained ANN applied to global scales where it showed reduced errors. Although both these methods were applied successfully to building an error regression model, they were limited to forested areas and/or coarse resolution, which do not represent the dense urban areas. Bagheri et al. (2018) fused two different sets of DEM data (TanDEM-X and Cartosat-1) using ANN to enhance the quality of both DEM datasets [18]. The authors trained an ANN to learn the pattern of the relationship between height errors and features from the two datasets. The relative accuracy of derived DEM was improved both DEMs up to 50% in the validation. The authors drew the usage of ANN with strength in pattern recognition, which is the core idea in this study for DEM enhancement. Figure 1 shows two main limitations of SRTM DEM: (1) as sensors partially do not penetrate the vegetation area, the top of the canopy level represents the elevation of the forested area; and (2) with its coarse resolution, it does not represent particularly the dense urban cities well—for example, a grid could present the average of elevations of a low lying road/area and high rise buildings within that grid. The impacts of these limitations can be significant, for example, inaccuracy of flood simulations that affect mitigation measures [19–21].

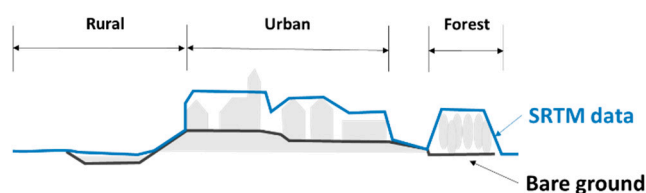


Figure 1. Limitations of Shuttle Radar Topography Mission (SRTM) digital elevation model (DEM) on the scanning of surface [22].

This paper presents significant improvements to the SRTM DEM using an ANN with remote sensing data. The improvement is particularly significant for dense urban areas. Figure 2 demonstrates the schematic diagram of our DEM improvement methodology. Generally, it requires four types of data; multispectral imagery, the DEM to be improved (SRTM DEM in this study), the building footprint for sorting the building areas, and a reference DEM (ground truth elevation).

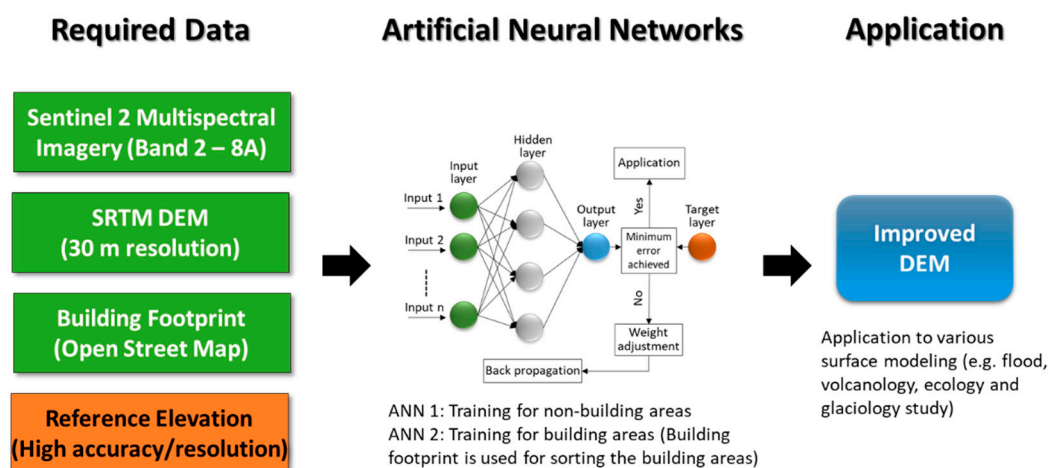


Figure 2. Schematic diagram of DEM improvement methodology.

Multispectral imagery is produced by the sensors which measure the reflected energy within several specific bands/sections of the electromagnetic spectrum. This can be defined as the acquisition of images in hundreds of contiguous, registered, spectral bands such that for each pixel a radiance spectrum can be derived [23–25]. Sentinel-2 multispectral imagery has 13 bands of wavelengths. In this study only eight bands, band 2–band 8A, are used while the remaining five bands (bands 1, 9, 10, 11 and 12) are not relevant in this study, as they are for aerosol, water vapor, snow, ice, and clouds correction [26]. Two sets of experiments with ANN training were conducted. One ANN was trained for non-building areas, while the other ANN was only for building areas. The high spatial resolution (1 m) and high-accuracy (40 cm) surveyed DEM was used as the reference elevation. Once the performance of the trained ANN was acceptable, it could be applied to areas where their SRTM DEMs are to be improved.

In this research, high-resolution and high-accuracy surveyed DEMs are available for Nice (France) and Singapore. The ground truth DEMs were used as reference DEMs to train and validate the ANN. SRTM DEM and Sentinel 2 data were used as common inputs for all areas. The trained ANN was later be applied to other areas in Nice and Singapore to verify its applicability. The performance of the DEM improvement scheme was evaluated over two dense urban cities using various matrices, e.g., visual clarity, scatter plots, root mean square error (RMSE), and flood maps.

2. Materials

2.1. SRTM DEM

SRTM DEM is an international joint project to collect three-dimensional digital mapping of over 80% of the Earth's surface (between 60° N and 56° S) collected in 2000, and it is available at no cost [27]. 3 arc-second resolution has been available since 2005 and 1 arc-second resolution for the globe was available after 2015. The performance requirements for the SRTM DEM data are such that the linear vertical absolute height error shall be less than 16 m and the relative height error shall be less than 10 m, for 90% of the data [5]. It should be noted, however, that its accuracy is limited to RMSE of approximately 14 m over Singapore's forest areas, due to C-band wavelengths that do not adequately penetrate the vegetation canopy [9]. Thus, the elevation in vegetation area presents an intermediate height between the top of the canopy and the bare surface. Also, due to its coarse resolution (~30 m since 2015; ~92 m prior to 2015), it does not present precise urban characteristics. In this study, SRTM DEM was selected to be improved using the DEM improvement scheme developed.

2.2. High-Accuracy and High-Resolution Surveyed DEM (Ground Truth)

High-resolution (1 m) and high-accuracy (40 cm) DEMs from Nice Côte d'Azur Metropolis (France) and Singapore's Building and Construction Authority (BCA) were used for training the ANN. Both DEMs were collected in 2014. The performance of the SRTM DEM and improved SRTM (iSRTM) DEM were evaluated using these ground truth data.

2.3. Sentinel 2 Multispectral Imagery

Sentinel 2 is an earth observation mission which was developed by the European Space Agency (ESA) as a part of the Copernicus Programme to perform terrestrial observations in support of services such as forest monitoring, land cover changes detection, and natural disaster management [25]. The Sentinel 2 multispectral instrument obtains the reflective wavelength of the multispectral observations with directional effects caused because of the reflectance anisotropy of the surface [28]. The multispectral imagery can be used for land use classification, for seasonal monitoring, and for agricultural and environmental applications [29–32]. Using different reflectance values from different land use types, the area can be classified by clustering and machine learning methods. Kim et al. (2018) analyzed the different reflectance of Sentinel 2 with different land uses [8]. The reflectance of short wave infrared (SWIR) bands (Bands 6–8) in forest areas is higher than that in urban areas; on the other hand, the reflectance of near infrared (NIR) bands (Bands 2–5) in urban areas is higher than that in the forest area. These different characteristics in each band help to classify land use in ANN as input nodes. These characteristics, together with SRTM DEM, have been fully utilized in this study to generate the improved SRTM DEM using an ANN. Table 1 shows the metadata of Sentinel 2 multispectral imagery for Nice, France and Singapore.

Table 1. Property of collected Sentinel 2 multispectral imagery.

Property	Nice, France	Singapore
Entity ID	L1C_T32TLP_A016836_20180912T103308	L1C_T48NUG_A004863_20180210T033204
Acquisition Date	2018-09-12	2018-02-10
Tile Number	T32TLP	T48NUG
Cloud Cover (%)	1.5258	5.6381
Platform	SENTINEL-2A	SENTINEL-2B
Processing Level	LEVEL-1C	LEVEL-1C

2.4. Artificial Neural Network

ANNs are one type of machine learning system. ANNs apply mathematical learning algorithms which are simulated by properties of the biological neural networks. ANNs are loosely based on biological neural networks in such a way that they are implemented as a system of interconnected processing elements which are functionally analogous to biological neurons. The connections between distinct layers have numerical values, called weights, and systematic altering of these values will give the ability to approximate the desired function [33].

An ANN is formed in three layers: input layer, hidden layer, and output layer. This traditional multiple layer perceptron (MLP) is a feed-forward neural network to generate the output from input data using a backpropagation algorithm [34]. The input layer has input neurons that transfer information via synapses to the hidden layer, and similarly the hidden layer transfers this information to the output layer via additional synapses. The synapses store values referred to as weights that help them to control the input and output to different layers. In mathematical terms, a computational neuron in the hidden or output layers can be described by the following equations:

$$u = \sum_{i=1}^n w_i x_i \quad (1)$$

and

$$y = \varphi(u + b) \quad (2)$$

where x_1, x_2, \dots, x_n are the input signals to the neuron, w_1, w_2, \dots, w_n are the synaptic weights, u is the linear combiner of the input signals, b is the bias, and y is the output signal of the neuron, whereas $\varphi(\cdot)$ is the activation function to limit the amplitude of the output signal and to create mapping between the input and output signals.

This study makes use of the strength of an ANN in pattern recognition and classification to build an error regression model to derive more accurate DEMs. The ANN is able to classify the areas based on their reflectance values and identify the general error pattern, and reduce the errors between elevations of the SRTM DEM and the reference DEM for different land uses from the training process.

3. Methodology

3.1. Data Pre-Processing

As all of the remote sensing and surveyed DEM data mentioned above have different resolutions (i.e., SRTM DEM 30 m; Sentinel 2 10–60 m; surveyed DEM 1 m), all input layers were standardized to a common resolution (10 m) using the nearest neighbor sampling method [35], as shown in Figure 3. This was also intended to downscale the SRTM 30 m to 10 m resolution as Sentinel 2 has 10 m resolution for its 4 bands (Band 2, 3, 4, 8). Due to the limitation of computing resources, this research did not consider resolutions finer than 10 m.

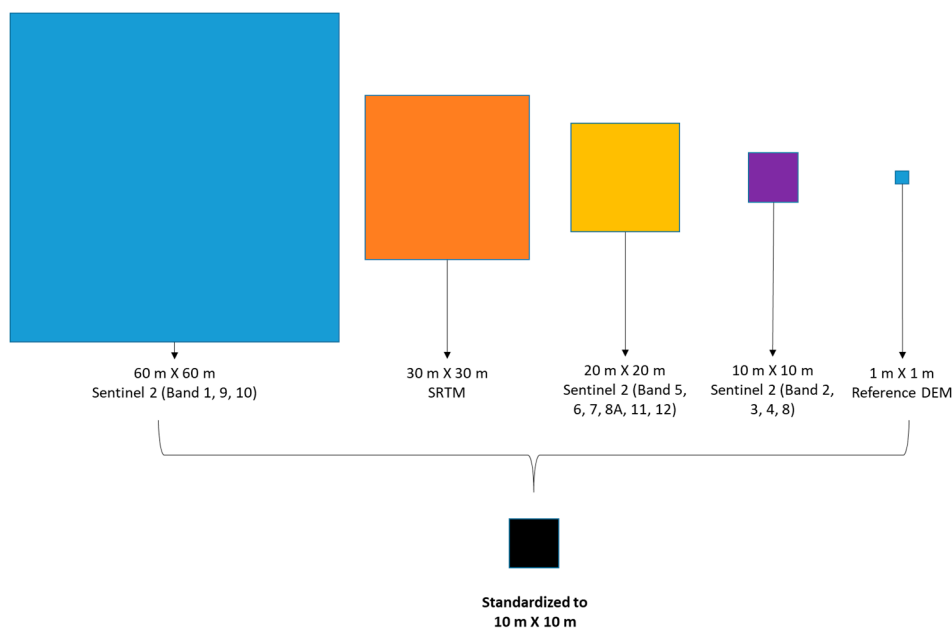


Figure 3. Standardization of different resolutions from different sources.

The selection of Sentinel 2 imagery was based on the least cloud presence, rather than the matching date of the data acquisition between SRTM DEM and Sentinel 2. This is because there is no matching period between the two (Sentinel 2 started from 2015 onward; SRTM started in the year 2000), while the presence of clouds in this case leads to the inaccuracy of the ground reflectance. The cloud filtering process in this study involved the screening of Sentinel 2 tile metadata to shortlist those that are attributed with a known cloud presence of less than 10%. From the shortlisted tiles, visual screening of the least cloud presence at the study area was carried out.

3.2. Artificial Neural Network Setup

Matlab Neural Network Toolbox was used to develop the DEM improvement scheme in this study. It provides a neural network to generalize nonlinear relationships between inputs and outputs using feed-forward networks. The feed-forward neural network is the first and simplest type of ANN devised [36]. It contains multiple neurons arranged in layers, and all of these neurons have the connections. The network with sigmoid activation function fits the multi-dimensional problems [37].

The network was trained with the Levenberg-Marquardt (LM) backpropagation algorithm to minimize the error using the mean squared error for the cost function [38,39]. This method is a standard technique for solving nonlinear least squares problems to fit a curve by minimizing the sum of the square of the errors between input and output nodes. The training was continued until the training error ceased to decrease or changed insignificantly. The trained ANN was then applied to the test data set. In this study, the data set was divided into 70% for training, 15% for an overfitting test, and 15% for independent testing of network performance. Table 2 shows the input, target, and output layers in the ANN. The reflectance values from Sentinel 2 bands and the elevation from SRTM DEM were placed in the input layer and the elevation of reference DEM was placed in the target layer. Two separate ANN trainings were used, one for buildings only and the other for the entire area without buildings. Buildings were classified with building footprints from the Open Street Map (OSM). The elevation of iSRTM DEM was then calculated from the process of ANN. The outputs from two ANNs were merged into one DEM. The neural network used in this research contained one hidden layer with 10 hidden neurons.

Table 2. Input, target, and output layers in ANN training.

Input Layer	Target Layer	Output Layer
Reflectance values of Sentinel 2, multispectral imagery SRTM DEM elevations	Surveyed DEM elevations	Improved (Rectified) elevations

4. Proof of Concept and Application of the Approach

This section evaluates the performance of the DEM derived using the method developed in this study, as described in Section 3. DEMs in Nice (France) and Singapore were taken into consideration. Two scenarios of test cases were introduced in dense urban areas: (1) the ANN model trained and validated in Nice, France; and (2) the ANN model trained in Nice and validated in Singapore. The second case was essential, as we needed to ascertain the applicability of the ANN model, trained in Nice, at other places where no high-quality DEM, except satellite imagery, is available.

For the case of urban areas in Nice, the training area has an area of 12.0 km² while the validation area was 5.2 km². Figure 4 shows the satellite image of the training (box with blue comb pattern) and validation (box with red comb pattern) areas. The areas are mainly urbanized with buildings, and the elevation profiles are from 0 m to 200 m. The average building height is 19.1 m (maximum 60.8 m) and buildings occupy 34% of the total area.

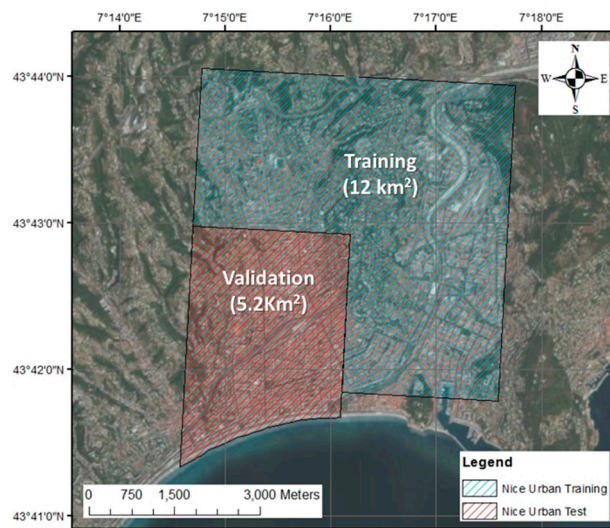


Figure 4. Training and validation areas in Nice: dense urban areas.

The ANN was trained in the training area with 1 m reference DEM data as the target layer. The iSRTM DEM was obtained from two ANN trainings, one with and one without building heights. The trained ANNs were then applied to the validation area and the performances were evaluated against the reference DEM. Figure 5 shows the comparison of elevation maps of various DEMs.

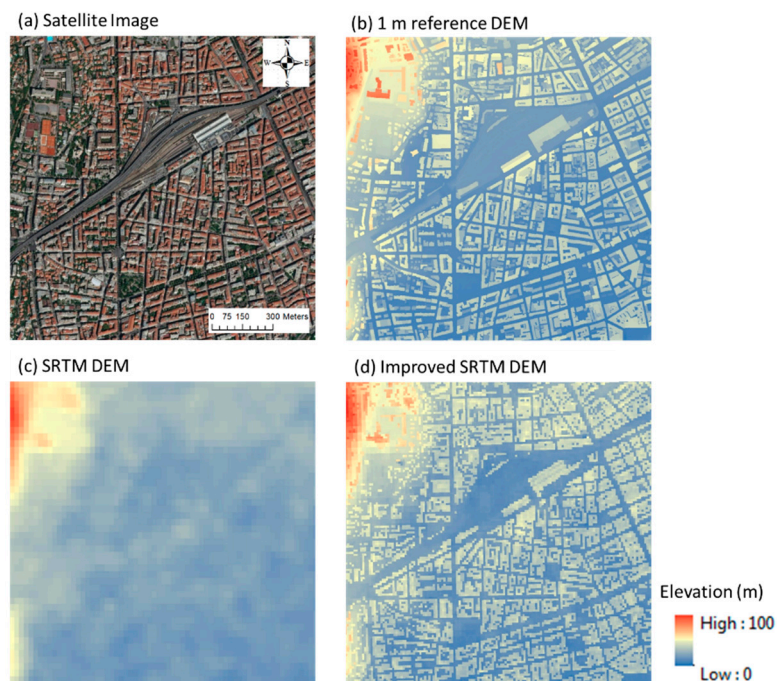


Figure 5. Comparisons of (a) satellite image, (b) 1 m reference DEM, (c) SRTM DEM and (d) improved SRTM (iSRTM) DEM in dense urban area in Nice.

Figure 5a is a satellite image of the test area depicting the land shapes; Figure 5b is the area from 1 m reference DEM; Figure 5c is the area from the original SRTM DEM with 30 m resolution; and Figure 5d is the area resulting from iSRTM DEM with 10 m resolution. The reference DEM shows most clear land shapes (i.e., buildings and roads); iSRTM DEM also shows clearer land shape visibility than the original SRTM DEM. iSRTM DEM (Figure 5d) most matched the reference DEM (Figure 5b). The significant improvements are reflected in statistical analysis in Figure 6 as well. The RMSE of iSRTM DEM reduced to 5.18 m from 8.36 m of SRTM DEM (a 38% reduction). Figure 6c shows

the frequency error distribution of iSRTM DEM and SRTM DEM. The percentage of absolute errors between -5 m to 5 m was 33.4% in SRTM DEM, while for iSRTM DEM it was 63.5%.

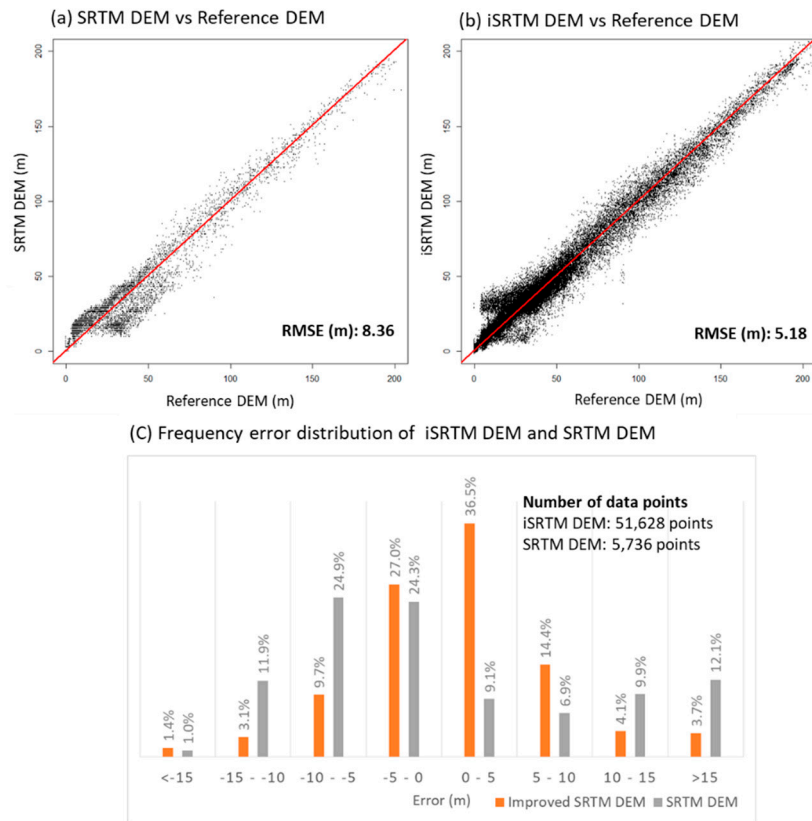


Figure 6. Scatter plots and RMSE comparisons between (a) SRTM DEM and (b) iSRTM DEM; frequency error distribution comparisons in dense urban area in Nice.

For the case of urban areas in Singapore, the interest was to investigate the quality of DEM generated by an ANN, trained in Nice, when it is applied in areas far away. The quality of DEM generated by the trained ANN was first validated in Singapore where good quality DEM is available. The area is a very dense urban area with high-rise buildings (Bukit Timah area, Singapore). The elevation ranges from 0 m to 100 m. The average building height is 18.8 m (maximum 90.5 m) and buildings occupy 28% of the total area.

Figure 7 shows a comparison of elevation maps between various DEMs. Figure 7a is a satellite image of the test area depicting the land shapes; Figure 7b shows the 1 m reference DEM; Figure 7c shows the original SRTM DEM with 30 m resolution; and Figure 7d shows the iSRTM DEM resulting from the ANN trained in Nice with 10 m resolution. The comparisons show that iSRTM DEM matches the 1 m reference DEM more than the original SRTM DEM. The improvements are reflected in statistical analysis in Figure 8 as well. The RMSE of iSRTM DEM is reduced from 10.70 m (SRTM DEM) to 6.93 m (35.2% reduction). Figure 8c shows the frequency error distribution of iSRTM DEM and SRTM DEM. The percentage of absolute errors between -5 m to 5 m was 14.9% in SRTM DEM, while for iSRTM DEM it was 49.3%.

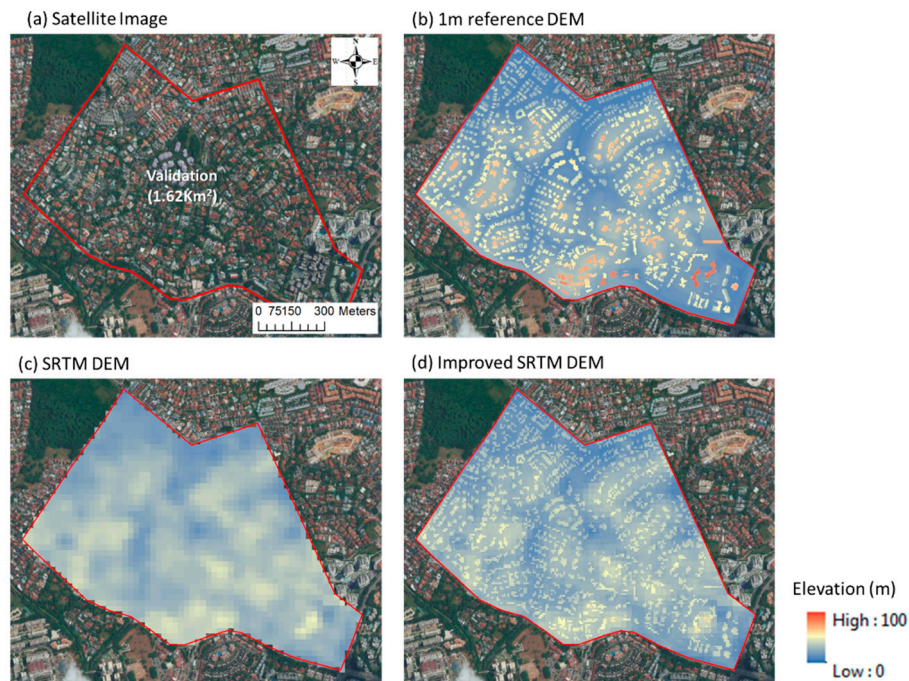


Figure 7. Comparisons of (a) satellite image, (b) 1 m reference DEM, (c) SRTM DEM, and (d) iSRTM DEM in dense urban area in Singapore.

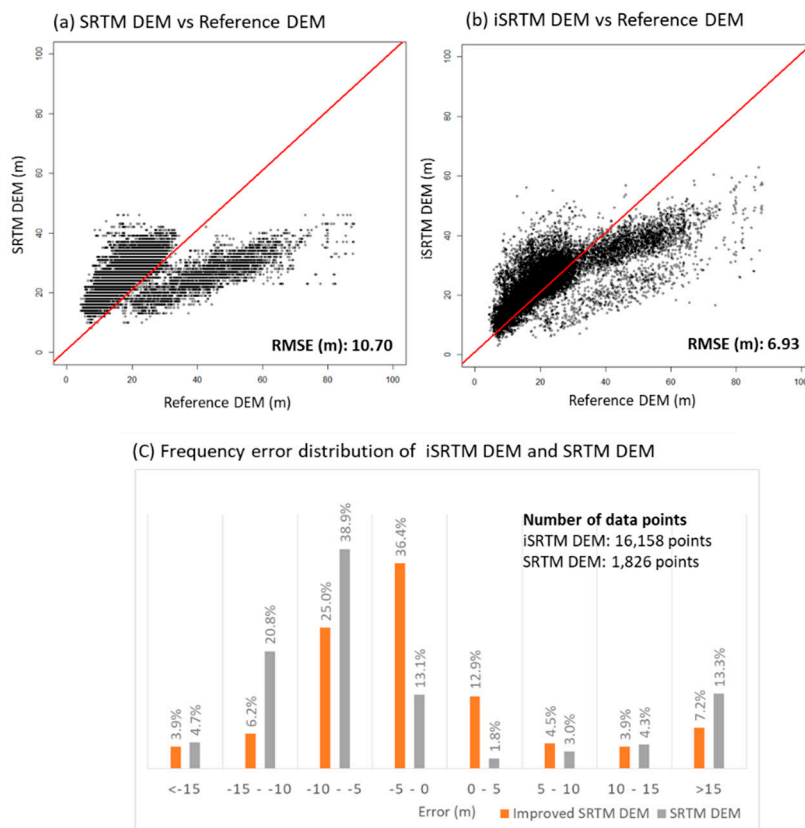


Figure 8. Scatter plots and root mean square error (RMSE) comparisons between (a) SRTM DEM and (b) iSRTM DEM; (c) frequency error distribution comparisons in dense urban area in Singapore.

Table 3 shows the error patterns in SRTM DEM and iSRTM DEM for different land-uses. The building areas in SRTM show the biggest RMSE, followed by impervious and pervious areas in

Nice and Singapore. The RMSE of all the different land-use areas were reduced in iSRTM DEM for both validation areas. The most improvement occurred in the impervious area of Nice with a 44.7% RMSE reduction, while building areas in Singapore showed the most RMSE reduction, with a 42% improvement. It would be interesting in future work to consider other error patterns, such as that in [40].

Table 3. The error patterns of SRTM DEM and iSRTM DEM in different land-uses.

Study Areas	RMSE of SRTM DEM (m)				RMSE of iSRTM DEM (m)			
	Entire	Impervious	Pervious	Buildings	Entire	Impervious	Pervious	Buildings
Nice, France	8.36	9.19	5.98	12.18	5.18	5.08	5.52	6.86
Singapore	10.70	11.49	9.46	16.45	6.93	7.42	6.16	9.53

It is an interesting finding that the SRTM DEM of a place, where no good-quality surveyed DEM is available, can still be significantly improved with ANN trained in a faraway dense urban area where high-quality ground truth data are available.

SRTM DEM and iSRTM DEM were used for flood modeling to verify the applicability of iSRTM DEM in the hydrodynamic modeling application. The MIKE 21 flow model developed by DHI Water & Environment [41] was used for a two-dimensional flow modeling system. The main purpose of this experiment was to identify which DEM represents the better fictitious flood maps based on common phenomena of inundation (flooding on low-lying areas such as roads in the urban areas). Fictitious rainfall (300 mm per 6 h) and a free flow boundary condition were used. The flood maps from different DEMs are compared in Figures 9 and 10.

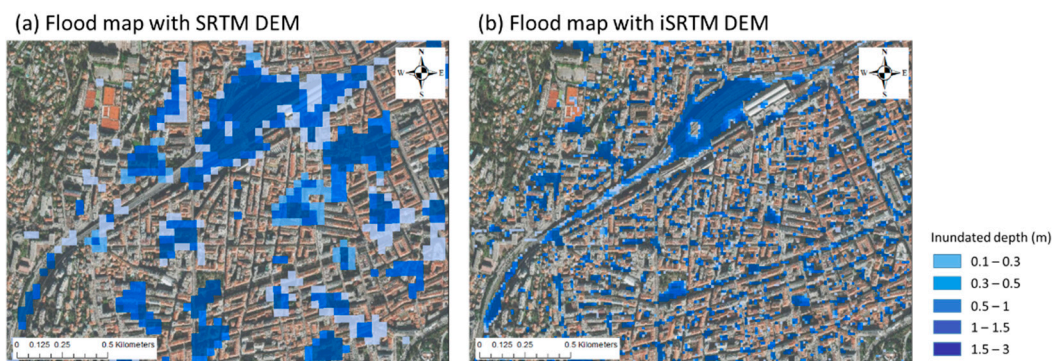


Figure 9. Flood map comparisons between (a) Flood map with SRTM DEM and (b) Flood map with iSRTM DEM in dense urban area of Nice, France.

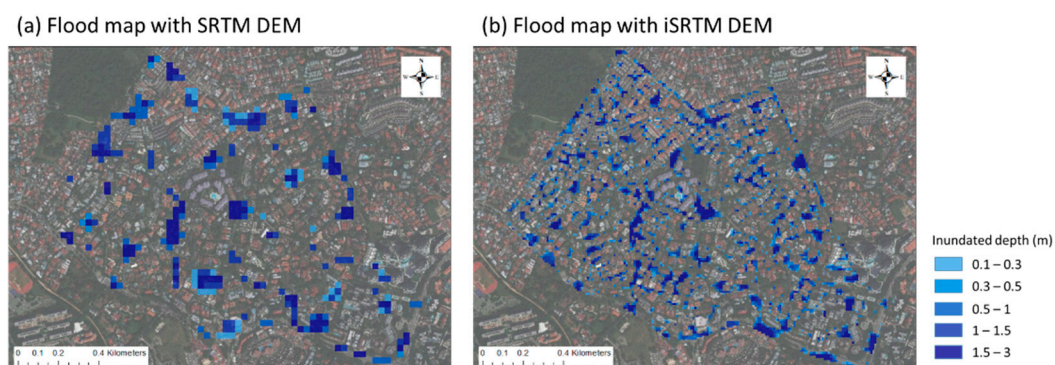


Figure 10. Flood map comparisons between (a) Flood map with SRTM DEM and (b) Flood map with iSRTM DEM in dense urban area of Singapore.

Figures 9 and 10 illustrate the inundated areas in Nice, France, and Singapore respectively. Different DEMs, SRTM DEM and iSRTM DEM, were used in the flood model to investigate the flood patterns. Flood maps resulting from iSRTM DEM capture the flooding in the flood prone areas, i.e., roads/low-lying areas, while flood maps resulting from the original SRTM DEM do not. Due to the coarse resolution of SRTM DEM (30 × 30 m) and inaccurate terrain elevation, flood patterns do not follow the real topographic characteristics.

5. Discussion

The main objective of this research was to develop the SRTM DEM improvement scheme using ANN along with other remote sensing data. As discussed in Section 1, SRTM has limitations due to its sensor and coarse resolution. The errors were able to be corrected using ANN with multispectral imagery after it was trained with ground truth data. This generalized neural network was applied to Singapore, which is far away from the training area in Nice France; as mentioned earlier the main purpose was to check whether the generated DEM in Singapore matches well with the surveyed DEM. Although the RMSE was significantly reduced, the building heights (higher than 60 m) did not clearly match with ground truth (Figure 7). The reason for this is that buildings in the study area of Nice are mostly less than 60 m (only 0.1% is between 60–100 m), which is not as high as Singapore's buildings (4% between 60–100 m). This means that the trained ANN mainly learned patterns of buildings of up to 60 m heights. Table 4 shows the percentage of impervious area and building characteristics in the study areas. This implies that the pattern of terrain shapes and building heights learned from similar areas and/or more variable patterns would generate better performance in improved SRTM.

Table 4. The percentage of impervious area and building characteristics in study areas.

Study Areas	Impervious Area (%)	Building Density (%)	Mean Building Height (m)	Percentage of Building Height in Different Ranges (%)		
				0–30 m	30–60 m	60–100 m
Nice, France	64.7	34.0	19.1	93.0	6.9	0.1
Singapore	62.5	28.0	18.8	84.1	11.9	4.0

The building areas were filtered using the Open Street Map (OSM) building footprint. It has been reported that OSM data may have some inaccuracy with its positioning in a few meters [42,43]. In this research, we used 10 m resolution for the DEM so that this error would not be significant. However, the presence of buildings in the data set is important, in that it is necessary to use the latest building information.

The 2D flood maps were generated using different DEMs with fictitious hydrologic data. Flood maps may be different from the actual situations as drainage networks are not considered. Also, this research did not use the actual rainfall characteristics of the areas. The flood maps from iSRTM DEM, however, showed that it captures the flooding on the roads (low-lying areas) better than that of SRTM DEM. This finding is not surprising, as the finer resolution iSRTM DEM (10 m) incorporates the terrain characteristics similar to those of the real condition.

The data fusion technique can be applied to this DEM improvement scheme using more data from other satellites (e.g., TanDEM-X, ASTER DEM, AW3D DEM, Landsat 8, Sentinel 1 and ASTER imagery). This technique would increase the performance of the output as the limitation of one sensor could be compensated by the other sensors [16]. Also, the methodology developed is quite flexible in data selection and can be applied to the other space-borne DEM data sources mentioned above for their improvement.

This study used a classical neural network regression method to reduce the error between ground truth data and SRTM. More complicated and different architecture of neural networks could allow improved performance by reducing errors.

6. Summary and Conclusions

A new DEM improvement scheme for SRTM DEM in dense urban cities was suggested and described in this paper. The scheme was developed using an artificial neural network (ANN) with SRTM DEM and Sentinel 2 multispectral imagery as the input nodes, while high resolution and accuracy surveyed DEM was used as the target layer. The trained ANN was able to classify the land-uses and land-covers with the assistance of different bands of Sentinel 2. Based on the various land characteristics in the training, different weights were calculated to reduce the errors between the elevations of SRTM DEM and surveyed DEM.

Two scenarios were taken into consideration for training and validation: (1) an ANN model trained and validated in Nice, France; and (2) an ANN model trained in Nice and validated in Singapore. In both scenarios the performance of improved SRTM (iSRTM DEM) was shown to be significantly better than its counterpart, SRTM DEM. In the dense urban city of Nice, the RMSE reduction of the iSRTM DEM was 38% and its visibility (land shapes, buildings and roads) was clearer than SRTM DEM. As one of the interests in the study was to improve the SRTM DEM of faraway locations, where no high-quality surveyed DEM is available, the ANN trained in Nice was used to generate the DEM of a dense urban area in Singapore to test its applicability (scenario 2). The test performance again showed significant improvement over SRTM DEM, with a RMSE reduction of 35.2%. It is interesting to note that a well trained ANN somewhere with a high-accuracy DEM can be applied to generate DEM at other far way places, so long as their patterns are similar to the pattern of the place where ANN is trained. Flood simulations were conducted using fictitious hydrological data and different topography from SRTM DEM and iSRTM DEM. Flood map resulting from iSRTM DEM captured better flooding on low-lying areas such as roads. The scheme developed is able to be used in hydrodynamic applications where topographical information is crucial.

This study has shown that the quality of SRTM DEM can still be significantly improved with the DEM improvement scheme proposed in this paper. The DEM improvement scheme can be applied to the areas where high-quality DEM is not available. Also, the improved SRTM can be used in many types of applications (i.e., flood, groundwater modeling) to allow the modeling performance to proceed with high confidence.

Author Contributions: Conceptualization, D.E.K. and S.-Y.L.; Methodology, D.E.K. and S.-Y.L.; Software, D.E.K.; Validation, D.E.K., S.-Y.L. and J.L.; Formal Analysis, D.E.K. and J.L.; Investigation, D.E.K. and P.G.; Resources, P.G. and L.A.; Data Curation, D.E.K.; Writing-Original Draft Preparation, D.E.K.; Writing-Review & Editing, S.-Y.L., P.G. and J.L.; Visualization, D.E.K. and J.L.; Supervision, S.-Y.L., P.G. and L.A.; Project Administration, D.E.K. and S.-Y.L. All authors have read and agree to the published version of the manuscript.

Funding: This research received no external funding.

Acknowledgments: We are very grateful to all those organizations which made their data available to us: (1) Métropole Nice Côte d'Azur and Building and Construction Authority of Singapore for providing the extremely high resolution DEMs of Nice, France and Singapore respectively; (2) National Aeronautics and Space Administration (NASA) for SRTM; (4) European Space Agency (ESA) for Sentinel-2; (5) OpenStreetMap for building foot prints; and (6) Willis Towers Watson for Research Network for making this study possible.

Conflicts of Interest: The authors declare no conflict of interest.

References

1. Moudrý, V.; Lecours, V.; Gdulová, K.; Gábor, L.; Moudrá, L.; Kropáček, J.; Wild, J. On the use of global DEMs in ecological modelling and the accuracy of new bare-earth DEMs. *Ecol. Model.* **2018**, *383*, 3–9. [[CrossRef](#)]
2. Favalli, M.; Fornaciai, A. Visualization and comparison of DEM-derived parameters. Application to volcanic areas. *Geomorphology* **2017**, *290*, 69–84. [[CrossRef](#)]
3. Wang, D.; Käab, A. Modeling Glacier Elevation Change from DEM Time Series. *Remote Sens.* **2015**, *7*, 10117–10142. [[CrossRef](#)]
4. Mirosław-Świątek, D.; Szporak-Wasilewska, S.; Michalowski, R.; Kardel, I.; Grygoruk, M. Developing an algorithm for enhancement of a digital terrain model for a densely vegetated floodplain wetland. *J. Appl. Remote Sens.* **2016**, *10*, 36013. [[CrossRef](#)]

5. Rodríguez, E.; Morris, C.S.; Belz, J.E. A Global Assessment of the SRTM Performance. *Photogramm. Eng. Remote Sens.* **2006**, *72*, 249–260. [[CrossRef](#)]
6. Zhang, W.; Montgomery, D.R. Digital elevation model grid size, landscape representation, and hydrologic simulations. *Water Resour. Res.* **1994**, *30*, 1019–1028. [[CrossRef](#)]
7. Moore, I.D.; Grayson, R.B.; Ladson, A. Digital terrain modelling: A review of hydrological, geomorphological, and biological applications. *Hydrol. Process.* **1991**, *5*, 3–30. [[CrossRef](#)]
8. Kim, D.; Sun, Y.; Wendi, D.; Jiang, Z.; Liong, S.-Y.; Gourbesville, P. Flood Modelling Framework for Kuching City, Malaysia: Overcoming the Lack of Data. In *Water Resources Quality and Management in Baltic Sea Countries*; Springer: Berlin/Heidelberg, Germany, 2018; pp. 559–568.
9. Wendi, D.; Liong, S.; Sun, Y.; Doan, C.D. An innovative approach to improve SRTM DEM using multispectral imagery and artificial neural network. *J. Adv. Model. Earth Syst.* **2016**, *8*, 691–702. [[CrossRef](#)]
10. Carabajal, C.C.; Harding, D.J. SRTM C-Band and ICESat Laser Altimetry Elevation Comparisons as a Function of Tree Cover and Relief. *Photogramm. Eng. Remote Sens.* **2006**, *72*, 287–298. [[CrossRef](#)]
11. Misra, P.; Avtar, R.; Takeuchi, W. Comparison of Digital Building Height Models Extracted from AW3D, TanDEM-X, ASTER, and SRTM Digital Surface Models over Yangon City. *Remote Sens.* **2018**, *10*, 2008. [[CrossRef](#)]
12. Gamba, P.D.A.; Houshmand, F.B. SRTM data characterization in urban areas. *Int. Arch. Photogramm. Remote Sens. Spat. Inf. Sci.* **2002**, *34*, 55–58.
13. Costantini, M.; Malvarosa, F.; Minati, E.; Zappitelli, E. A Data Fusion Algorithm for DEM Mosaicking: Building a Global DEM with SRTM-X and ERS Data. In Proceedings of the 2006 IEEE International Symposium on Geoscience and Remote Sensing, Denver, CO, USA, 31 July–4 August 2006; pp. 3861–3864.
14. Yamazaki, D.; Ikeshima, D.; Tawatari, R.; Yamaguchi, T.; O’Loughlin, F.E.; Neal, J.C.; Sampson, C.; Kanae, S.; Bates, P.D. A high-accuracy map of global terrain elevations. *Geophys. Res. Lett.* **2017**, *44*, 5844–5853. [[CrossRef](#)]
15. Yue, L.; Shen, H.; Liu, L.; Yuan, Q.; Zhang, L. A Global Seamless DEM Based on Multi-Source Data Fusion (GSDEM-30): Product Generation and Evaluation. *Preprints* **2019**. [[CrossRef](#)]
16. Muhadi, N.A.; Kassim, M.S.M.; Abdullah, A.F. Improvement of Digital Elevation Model (DEM) using data fusion technique for oil palm replanting phase. *Int. J. Image Data Fusion* **2018**, *10*, 232–243. [[CrossRef](#)]
17. Kulp, S.A.; Strauss, B.H. CoastalDEM: A global coastal digital elevation model improved from SRTM using a neural network. *Remote Sens. Environ.* **2018**, *206*, 231–239. [[CrossRef](#)]
18. Bagheri, H.; Schmitt, M.; Zhu, X. Fusion of TanDEM-X and Cartosat-1 elevation data supported by neural network-predicted weight maps. *ISPRS J. Photogramm. Remote Sens.* **2018**, *144*, 285–297. [[CrossRef](#)]
19. Hawker, L.; Bates, P.; Neal, J.; Rougier, J. Perspectives on Digital Elevation Model (DEM) Simulation for Flood Modeling in the Absence of a High-Accuracy Open Access Global DEM. *Front. Earth Sci.* **2018**, *6*, 233. [[CrossRef](#)]
20. Fewtrell, T.J.; Bates, P.D.; Horritt, M.; Hunter, N.M. Evaluating the effect of scale in flood inundation modelling in urban environments. *Hydrol. Process.* **2008**, *22*, 5107–5118. [[CrossRef](#)]
21. Hunter, N.M.; Bates, P.D.; Néelz, S.; Pender, G.; Villanueva, I.; Wright, N.; Liang, D.; Falconer, R.A.; Lin, B.; Waller, S.; et al. Benchmarking 2D hydraulic models for urban flooding. *Proc. Inst. Civ. Eng. Water Manag.* **2008**, *161*, 13–30. [[CrossRef](#)]
22. Radiomobile. Background on DEM. Available online: radiomobile.pe1mew.nl/?Geodata:Background_on_DEM (accessed on 3 March 2020).
23. Goetz, A.F.; Vane, G.; Solomon, J.E.; Rock, B.N. Imaging Spectrometry for Earth Remote Sensing. *Science* **1985**, *228*, 1147–1153. [[CrossRef](#)]
24. Rencz, A.N.; Bowie, C.; Ward, B.C. Application of thermal imagery from LANDSAT data to locate kimberlites, Lac de Gras area, district of Mackenzie, N.W.T. In *Searching for Diamonds in Canada: Geological Survey of Canada, Open File 3228*; Geological Survey of Canada: Ottawa, ON, Canada, 1996; pp. 255–257.
25. Drusch, M.; Del Bello, U.; Carlier, S.; Colin, O.; Fernandez, V.; Gascón, F.; Hoersch, B.; Isola, C.; Laberinti, P.; Martimort, P.; et al. Sentinel-2: ESA’s Optical High-Resolution Mission for GMES Operational Services. *Remote Sens. Environ.* **2012**, *120*, 25–36. [[CrossRef](#)]
26. Gatti, A.; Bertolini, A. Sentinel-2 Products Specification Document. Available online: <https://sentinel.esa.int/web/sentinel/document-library/content/-/article/sentinel-2-level-1-to-level-1c-product-specifications> (accessed on 3 March 2020).

27. U.S. Geological Survey (USGS). Available online: https://www.usgs.gov/centers/eros/science/usgs-eros-archive-digital-elevation-shuttle-radar-topography-mission-srtm-1-arc?qt-science_center_objects=0#qt-science_center_objects (accessed on 3 March 2020).
28. Roy, D.P.; Li, J.; Zhang, H.K.; Yan, L.; Huang, H.; Li, Z. Examination of Sentinel-2A multi-spectral instrument (MSI) reflectance anisotropy and the suitability of a general method to normalize MSI reflectance to nadir BRDF adjusted reflectance. *Remote Sens. Environ.* **2017**, *199*, 25–38. [[CrossRef](#)]
29. Andres, L.; Salas, W.A.; Skole, D. Fourier analysis of multi-temporal AVHRR data applied to a land cover classification. *Int. J. Remote Sens.* **1994**, *15*, 1115–1121. [[CrossRef](#)]
30. Ashish, D.; McClendon, R.W.; Hoogenboom, G. Land-use classification of multispectral aerial images using artificial neural networks. *Int. J. Remote Sens.* **2009**, *30*, 1989–2004. [[CrossRef](#)]
31. Moody, D.; Brumby, S.P.; Rowland, J.C.; Altmann, G.L. Land cover classification in multispectral imagery using clustering of sparse approximations over learned feature dictionaries. *J. Appl. Remote Sens.* **2014**, *8*, 84793. [[CrossRef](#)]
32. Pande, C.B.; Moharir, K.N.; Khadri, S.F.R.; Patil, S. Study of land use classification in an arid region using multispectral satellite images. *Appl. Water Sci.* **2018**, *8*, 123. [[CrossRef](#)]
33. Gurney, K. *An Introduction to Neural Networks*; UCL Press: London, UK, 1997; ISBN 978-1-85728-673-1.
34. Seiffert, U. *Multiple Layer Perceptron Training Using Genetic Algorithms*; ESANN: Bruges, Belgium, 2001.
35. Takagi, M. Accuracy of digital elevation model according to spatial resolution. *Int. Arch. Photogramm. Remote Sens.* **1998**, *32*, 613–617.
36. Schmidhuber, J. Deep learning in neural networks: An overview. *Neural Netw.* **2015**, *61*, 85–117. [[CrossRef](#)]
37. Han, J.; Moraga, C. The influence of the sigmoid function parameters on the speed of backpropagation learning. In *From Natural to Artificial Neural Computation*; Springer: Berlin/Heidelberg, Germany, 1995.
38. Levenberg, K. A method for the solution of certain non-linear problems in least squares. *Q. Appl. Math.* **1944**, *2*, 164–168. [[CrossRef](#)]
39. Marquardt, D.W. An Algorithm for Least-Squares Estimation of Nonlinear Parameters. *J. Soc. Ind. Appl. Math.* **1963**, *11*, 431–441. [[CrossRef](#)]
40. Hawker, L.; Rougier, J.; Neal, J.C.; Bates, P.D.; Archer, L.; Yamazaki, D. Implications of Simulating Global Digital Elevation Models for Flood Inundation Studies. *Water Resour. Res.* **2018**, *54*, 7910–7928. [[CrossRef](#)]
41. DHI, MIKE FLOOD. Available online: <https://www.mikepoweredbydhi.com/download/product-documentation> (accessed on 3 March 2020).
42. Brovelli, M.A.; Zamboni, G. A New Method for the Assessment of Spatial Accuracy and Completeness of OpenStreetMap Building Footprints. *ISPRS Int. J. Geo-Information* **2018**, *7*, 289. [[CrossRef](#)]
43. Fan, H.; Zipf, A.; Fu, Q.; Neis, P. Quality assessment for building footprints data on OpenStreetMap. *Int. J. Geogr. Inf. Sci.* **2014**, *28*, 700–719. [[CrossRef](#)]



© 2020 by the authors. Licensee MDPI, Basel, Switzerland. This article is an open access article distributed under the terms and conditions of the Creative Commons Attribution (CC BY) license (<http://creativecommons.org/licenses/by/4.0/>).